Dual wavelength evanescent coupler for nonlinear GaP-based microdisk resonators

Alejandro Lorenzo-Ruiz, Charles Cornet, Alexandre Beck, Yoan Léger

Research Article Vol. 3, No. 1 / 15 January 2020 / OSA Continuum 43

Dual wavelength evanescent coupler for nonlinear GaP-based microdisk resonators

ALEJANDRO LORENZO-RUIZ, CHARLES CORNET, ALEXANDRE BECK, AND YOAN LÉGER*

Univ Rennes, INSA Rennes, CNRS, Institut FOTON – UMR 6082, F-35000 Rennes, France
**yoan.leger@insa-rennes.fr*

Abstract: Wavelength conversion is one of the most demanded features in integrated photonics. During the last decade, second harmonic generation (SHG) in III-V semiconductor microdisks has been demonstrated to be an efficient way to achieve such conversion with particularly compact devices. Optimized coupling of both wavelengths to these devices still remains as a challenge. Here we compare three different approaches for vertical coupling between integrated waveguides and a III-V microdisk resonator in which SHG occurs: two well-established schemes and a new one using a single slit waveguide as an evanescent coupler.

The investigation of nonlinear processes within on-chip photonic devices has recently opened the door to a new whole category of functionalities from on-chip optical signal processing [1] to novel light sources [2] and sensors [3].

Among these nonlinear devices, wavelength converters appear as key components for data routing inside and outside the chip or to access wavelength ranges of interest for sensing. A usual configuration for such wavelength conversion is the use of second order nonlinear microdisk resonators. They offer highly confined whispering gallery modes (WGMs) [4] and the possibility of different phase matching schemes, from modal phase matching [5,6] to strict $\bar{4}$-phase-matching [7,8] allowing the possibility of achieving high efficiencies [9,10]. III-V semiconductors are one of the best candidates for this optical and integrable configurations [11] and among them, gallium phosphide (GaP) with a large indirect band-gap of 2.24eV, high transparency in the IR spectrum and high nonlinear susceptibility appears as a promising material for this kind of devices.

However, efficient coupling to octave-separated signals in a compact, microscale resonator remains challenging. Seminal works on second harmonic generation in III-V microdisks were carried out using a single tapered fiber as a coupler [12]. If tuning is the great asset of this technique, the alignment and distance between the fiber and the microdisk are hardly controlled and a strong mismatch between the fiber and resonator propagation constants severely impacts the coupling. Moreover, this scheme also strongly limits on-chip integration.

Integrated evanescent coupling schemes have thus progressively emerged [13] from lateral [4,11] to vertical coupling [14,15] with straight waveguides or curved ones (so-called pulley coupler) [16,17]. While the latter case is well adapted to large microresonators, where it does not impact strongly the physics within the resonators and offers high coupling efficiency [6,18], it can hardly fit few-microns large microdisk resonators. On the other side, short length evanescent coupling to a straight waveguide is much less tolerant to technological flaws. Huge technological effort is now dedicated to the optimization of such couplers, especially when considering signals with large spectral separation such as a whole octave [10,16,17]. If the add-drop configuration seems practically the most convenient solution as it allows to address independently the issues of propagation constant mismatch and mode engineering for the two wavelengths, one can still question the relevance of the less-perturbative all-pass configuration for dual-wavelength conversion.

#378654 https://doi.org/10.1364/OSAC.3.000043
Journal © 2020 Received 3 Oct 2019; revised 15 Nov 2019; accepted 19 Nov 2019; published 9 Jan 2020

OSA CONTINUUM

In this work we investigate theoretically the advantages and drawbacks of different coupling schemes for dual wavelength conversion into a microdisk resonator. We restrict ourselves to the case of SHG in zinc-blende semiconductor microdisk where strict $\bar{4}$ quasi-phase matching ($\bar{4}$ QPM) leads to the use of TE polarized modes as the input fundamental signal and TM polarized modes for the second harmonic. In this framework, vertical coupling is particularly convenient as it favors the coupling to TM output modes due to their large vertical evanescent tail. We thus consider a 3D bonded-membranes platform featuring two layers of photonic circuits, one for the waveguides and one for the microdisk. Both layers are made of the same material, namely GaP, to avoid large propagation constant mismatch. The three coupling configurations under scrutiny are the all-pass and add-drop configurations and a more original one based on a slit waveguide coupler (see Fig. 1 a to c). In a slit waveguide, the modes of two nearby waveguides couple into supermodes [19]. For small gap between the waveguides, TE-polarized symmetric supermodes are mainly trapped inside the slit while TM-polarized supermodes propagate through the waveguides as shown in Fig. 1 d. Modifying the gap width between the guides mainly affects the propagation constant of the TE modes. Hence it allows an independent tuning of the propagation constants (β) for the input TE and the output TM modes, similarly to the add-drop scheme. On the other hand, it only represents a single perturbation for the WGMs in the resonator like the all-pass coupler.

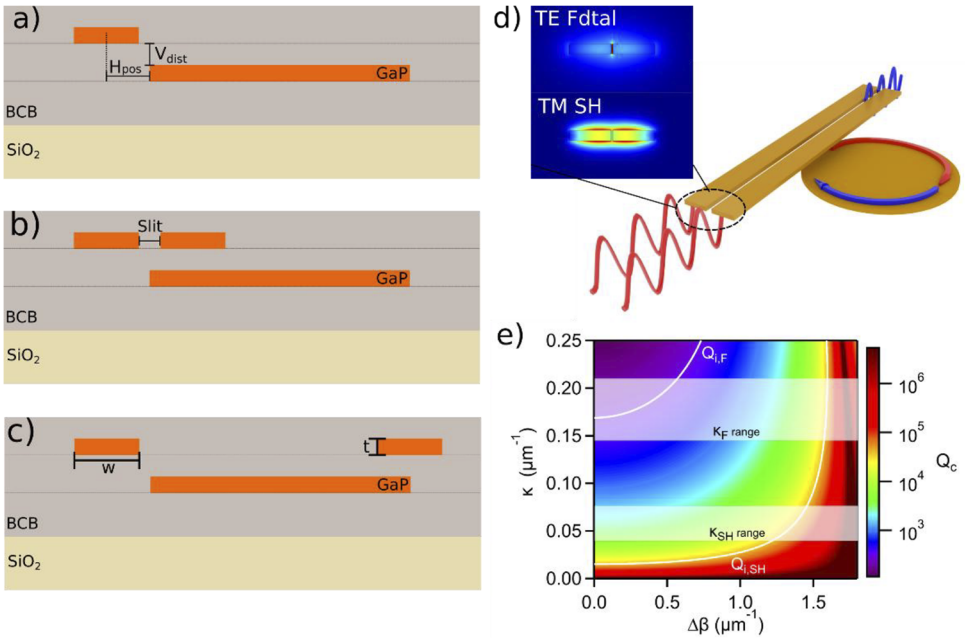

Fig. 1. (a, b, c) Schematic representation of the three models studied, all-pass, slit and add-drop configurations. (d) 3D model of the integrated system studied and modal profiles of the selected TE (top) and TM (bottom) selected symmetric supermodes of the slit waveguide. (e) Color plot of the coupling Q factor versus propagation constant mismatch and evanescent coupling coefficient κ between guide mode and WGM. Also indicated the intrinsic Q factor of the chosen disk at both frequencies and the κ range of the geometries simulated.

These three coupling schemes are compared, accounting for the same technological limitations of the 3D photonic platform of interest. The quality factors and the coupling regimes (under- or over-coupling) have been calculated at both fundamental and SH wavelengths for the three

OSA CONTINUUM

coupling schemes. They are then discussed in the framework of continuous and pulsed injection configurations.

The practical SHG configuration used to study the different coupling schemes allows wavelength conversion from ~2μm to ~1μm with a 180nm-thick microdisk with a radius of 3.4μm as previously reported in Ref. [8]. The modes are chosen to satisfy strict $\bar{4}$-QPM without requiring additional modal phase matching so that planar and radial numbers are equal to one for both frequencies and the azimuthal numbers (m) are respectively 18 and 38 for fundamental and second harmonic wavelengths in order to satisfy $\Delta m = m_{SH} - 2m_{fdtal} = \pm 2$. Figure 1(a,b,c) shows the important features of the technological platform and of the different coupling configurations. The two GaP membranes are encapsulated into BCB and integrated onto an optically thick SiO_2 layer lying on a silicon substrate (not represented in Fig. 1). We consider that the two GaP membranes can feature different thicknesses since they result from distinct technological steps. Parameters "w" and "t" are respectively the width and thickness of the coupling waveguide, "Hpos" is the distance between the edge of the microdisk and the centre of a waveguide, "Vdist" is the vertical distance between the microdisk and the waveguide layer and "s" is the width of the slit for the homonymous case. Refractive indices for materials come from [20,21].

We coupled semi-analytical description and 3D FEM and FDTD models to investigate the propagation through the investigated geometries at fundamental and SH wavelengths to characterize the resonances. In the numerical simulations, the Q-factors for the SH have been artificially limited by introducing additional losses in GaP to avoid extremely long computation times.

To describe the model theoretically, in first approximation, the evanescent coupling phenomenon can be analytically described by the coupled mode theory, through the system:

$$\frac{d}{dz}\begin{pmatrix} A \\ B \end{pmatrix} = \begin{pmatrix} 0 & i\kappa \exp(i\Delta\beta z) \\ i\kappa \exp(-i\Delta\beta z) & 0 \end{pmatrix}\begin{pmatrix} A \\ B \end{pmatrix} \tag{1}$$

where A and B are the field envelopes within the waveguide and the disk, κ is the cross-coupling coefficient, accounting for the mode overlap and $\Delta\beta$ is the propagation constant mismatch between the waveguide and WG modes. The coupling efficiency results from the integration of this system along the interaction length of the coupler. A non-zero value of $\Delta\beta$ is commonly associated with a decrease of the coupling. The situation is in reality more complex and depends on the value of the evanescent coupling parameter κ. To account for this dependence, we numerically assessed the coupling Q factor as a function of the β mismatch and the coupling parameter κ in Fig. 1d). The values of κ for the geometrical parameters of the present work lay between 0.14 and 0.22 μm^{-1} for the fundamental mode and between 0.04 and 0.07 μm^{-1} for the SH mode. These ranges are pointed out in the figure as well as the intrinsic Q factors values of both fundamental and SH resonances, allowing the reader to discriminate the areas of the color plot where overcoupling or undercoupling is achieved. As far as undercoupling regime is considered, a zero β mismatch always optimizes the coupling. On the contrary, in the overcoupling regime, a non-zero β mismatch can improve the coupling towards critical coupling condition. For the fundamental mode, this optimization can be practically achieved with reasonable values of $\Delta\beta$ but not for the SH mode.

We chose to compare the three coupling schemes through the assessment of their coupling quality factor Q_c and the overall conversion efficiency. The resonances of any WGM resonator are submitted to losses such as bending losses and material absorption. The linewidth and frequency of the resonance allow to define its intrinsic Q-factor Qi. When coupled to an access waveguide, the WGM resonances enlarge due to the additional losses induced by the coupling. The so-called loaded Q-factor Q_L of the coupled resonance can be expressed as $1/Q_L = 1/Q_i + 1/Q_c$, where Q_c is defined as the coupling Q-factor, depending on κ, $\Delta\beta$ and the effective interaction length of

OSA CONTINUUM

the coupler. The critical, under- and over-coupling regimes are defined by the relative values of Q_c and Q_i [22]. These coupling regimes are crucial parameters for wavelength conversion at both fundamental and SH wavelengths since they impact strongly the nonlinear configuration that one will observe within the resonator from weakly to highly depleted pump configurations [23]. When trying to maximize SHG, critical coupling may not be the optimal one [14]. To measure Q_c for the different schemes, the intrinsic Q-factor was calculated through FEM on the isolated microdisk while the loaded Q-factor was estimated by FDTD simulations through the measurement of the calculated resonance linewidths.

The geometrical parameters of the waveguides have been optimized for all three configurations to achieve $\Delta\beta$=0 for fundamental mode, SH mode, or both. These optimized parameters are provided in Table 1. Note that the values provided here for the all-pass configuration provides zero β mismatch only on the SH. The dispersion curves for the different waveguides are plotted in Fig. 2 and compared to the effective dispersion relation of the microdisk WGMs. The effective WGM propagation constant is calculated through the relation $\beta = m/R_{WGM}$ where R_{WGM} is the effective radius of the WGM [24]. For a single waveguide optimized for fundamental wavelength coupling, we observe a crossing point with the WGM at 2μm. In this case, zero β mismatch cannot be achieved close to 1 μm on TM modes and we find a mismatch of 4.15%. Similarly, when optimizing the waveguide for the SH coupling, the crossing point of the waveguide dispersion with the fundamental WGM resonance is made impossible, with 8.3% of mismatch. Using two distinct waveguides for the coupling of fundamental and SH modes (add-drop configuration) straightforwardly solves the zero β mismatch issue at the desired wavelengths. However, one can still observe that the group velocity of the waveguides does not match the one of the effective WGM dispersion, which will impose less tolerance against geometry deviation. Typical fabrication flaws in the order of 5% can be considered to account for film thickness variations due to local strain relaxation in the epitaxial layers, as well as lithography or etching-induced deviations onto the width of the waveguides or the slit opening. We numerically assessed that such flaws do not change the propagation constants by more than 1% for the three coupling cases making the three of them viable technologically.

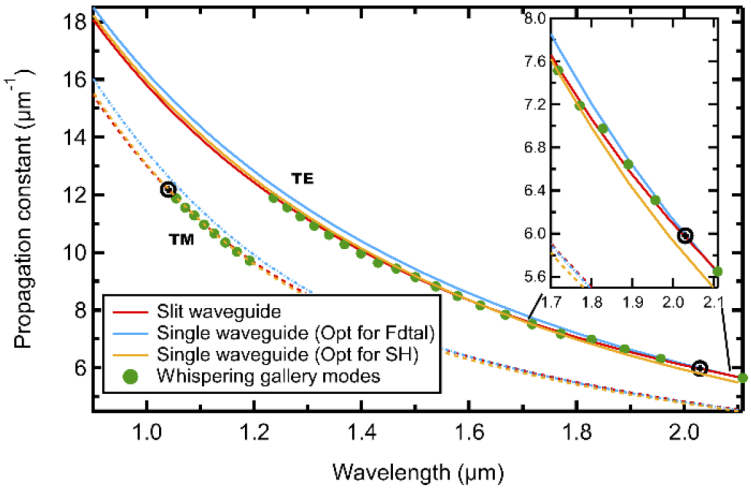

Fig. 2. Dispersion curves for the different configurations for both modes. TE (solid line) and TM (dashed line) between 0.9 and 2.1 μm. Black markers show the chosen WGMs for SHG

The additional degree of freedom provided by the slit geometry enables a more accurate and independent tuning of the TE and TM dispersion curves to match the effective dispersion of

OSA CONTINUUM

Table 1. Geometrical parameters of the different configurations for the β matching condition

	All-pass	Add-drop(F/SH)	Slit(s = 50nm)
Width	820nm	1000/820nm	700nm
Thickness	167nm	167nm	165nm
V_{dist}	400nm	400nm	400nm
H_{pos}	0nm	0/200nm	350nm

the microdisk. We not only get a zero β mismatch at the two wavelengths of interest but also a good group velocity matching in these spectral ranges (close-up view in Fig. 2). This property makes the geometry more tolerant to parameter deviations such as slight changes on the disk radius that shift the resonances. It also opens the path towards other applications like tunable wavelength conversion in the second [25] or third order regime [16] where phase matching is partially relaxed or less restrictive. Finally, when generating octaves of frequency combs an efficient coupling over a large spectral bandwidth is mandatory.

We now compare the three coupling schemes optimized for zero β mismatch (at SH wavelength for the all-pass configuration) in terms of Q-factors. The resonance profiles for both wavelengths and for each coupling schemes are plotted in Fig. 3, allowing to calculate the loaded Q-factors in each case. Due to the small size of the microdisk imposed by strict $\bar{4}$-QPM, the intrinsic Q-factor for the fundamental mode is very small: $Q_{i,F}$=295. On the contrary, the SH mode Q-factor is large and limited here by artificial absorption losses introduced in the calculation: $Q_{i,SH}$=39000. The consequence of the large value for $Q_{i,F}$ is that undercoupling is found for both the all-pass and add-drop configurations, resulting in a coupling Q-factor in the order of 500. The transmission depth is slightly better for the all-pass configuration due to the absence of drop port. In fact, drop port for the SH even needs to be moved aside from the microdisk by 200nm in the add-drop configuration to limit this transmission depth reduction. For the slit waveguide, overcoupling is observed (Q_c=160). For the vertical spacing of 400nm used in this work, the all-pass and add-drop configurations are thus more adapted to continuous wavelength conversion while the slit-waveguide is better suited to pulsed excitation regime as pointed out recently [14].

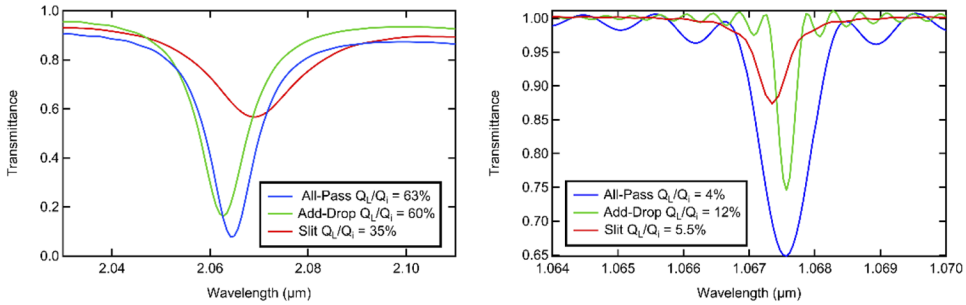

Fig. 3. Transmission spectra in all configurations for fundamental (left) and second harmonic (right) wavelengths. Legend shows the ratio between loaded and intrinsic quality factors, which is 50% at critical coupling.

For the second harmonic case, with a much higher intrinsic Q-factor, all three configurations are in overcoupling regime as indicated by the small loaded Q-factors and transmission depth below 0.5. Since the SH drop-port has been moved aside from the microdisk in the add-drop configuration to prevent unintentional coupling of the fundamental mode in this port, loaded Q-factor of the SH mode is enhanced in comparison with the all-pass case but the transmission depth is also reduced because of the smaller mode overlap. The coupling Q-factors on the SH

OSA CONTINUUM

modes are 1625 and 5300 for the all-pass and add-drop configuration respectively. The add-drop will thus be better adapted to continuous signal conversion while the all-pass shows particularly good specifications for wavelength conversion in the pulsed regime. For the slit waveguide configuration, a loaded Q factor comparable to the one of the all-pass is observed but at the expense of a strong reduction on the transmission depth, this necessarily comes from an increase of the losses in the microdisk, due to insertion losses and scattering towards other supermodes of the slit waveguide. If this should not affect too much the efficiency of the doubly resonant nonlinear process, it will be detrimental for the extraction of the SH mode by a factor of three compared to the all-pass case.

With the calculated quality factors, we can derive the theoretical overall conversion efficiency in continuous mode operation for the three cases, as described in Ref. [26,27]. It is important to note that these results cannot be extrapolated to the pulsed regime where a dynamical analysis would be required. The obtained results are presented in Table 2 where we notice that the add-drop configuration is 3 times more efficient than the all-pass case, and the slit configuration stays as an intermediate point. Despite the low Q factors of the fundamental mode, resulting from the reduced disk thickness required for strict $\bar{4}$-QPM, one obtains higher efficiencies (up to one order of magnitude) than the case of modal+$\bar{4}$-QPM reported in the literature (4×10^{-6} mW^{-1}at 1mW), when comparing theoretical predictions in the same operation conditions [5,25]. In the present case, the smaller Q factors can thus be considered as an asset to compensate the deviation from perfect double resonance condition.

Table 2. Absolute efficiencies calculated for the schemas for 1mW of pump.

	All-pass	Add-drop	Slit
η (mW^{-1})	3.14×10^{-5}	9.13×10^{-5}	4.06×10^{-5}

As a conclusion, we have investigated theoretically the characteristics of three different coupling schemes for a wavelength converter based on SHG in a III-V semiconductor microdisk integrated into a 3D photonic circuit architecture allowing for vertical coupling. We demonstrated that the add-drop coupling configuration is practically the most adapted configuration for conversion of continuous wave signals since it guarantees coupling regimes as close as possible to the critical case. On the opposite, the all-pass and the proposed slit waveguide configuration both appear as attractive coupling schemes for pulsed regimes. Moreover, the slit waveguide coupling scheme also allows matching of the group velocities of octave-split wavelengths which can be convenient for advanced tuning schemes of nonlinear processes or frequency comb spectral translation.

Funding

Agence Nationale de la Recherche (ANR-17-CE24-0019-01); Région Bretagne; Ministère de l'Enseignement Supérieur et de la Recherche.

Disclosures

The authors declare no conflicts of interest.

References

1. C. Koos, P. Vorreau, T. Vallaitis, P. Dumon, W. Bogaerts, R. Baets, B. Esembeson, I. Biaggio, T. Michinobu, F. Diederich, W. Freude, and J. Leuthold, "All-optical high-speed signal processing with silicon–organic hybrid slot waveguides," Nat. Photonics **3**(4), 216–219 (2009).
2. J. S. Levy, A. Gondarenko, M. A. Foster, A. C. Turner-Foster, A. L. Gaeta, and M. Lipson, "CMOS-compatible multiple-wavelength oscillator for on-chip optical interconnects," Nat. Photonics **4**(1), 37–40 (2010).
3. T. Baehr-Jones, M. Hochberg, G. Wang, R. Lawson, Y. Liao, P. A. Sullivan, L. Dalton, A. K.-Y. Jen, and A. Scherer, "Optical modulation and detection in slotted Silicon waveguides," Opt. Express **13**(14), 5216–5226 (2005).

OSA CONTINUUM

4. N. Thomas, R. J. Barbour, Y. Song, M. L. Lee, and K.-M. C. Fu, "Waveguide-integrated single-crystalline GaP resonators on diamond," Opt. Express **22**(11), 13555 (2014).
5. D. P. Lake, M. Mitchell, H. Jayakumar, L. F. dos Santos, D. Curic, and P. E. Barclay, "Efficient telecom to visible wavelength conversion in doubly resonant gallium phosphide microdisks," Appl. Phys. Lett. **108**(3), 031109 (2016).
6. A. W. Bruch, X. Liu, X. Guo, J. B. Surya, Z. Gong, L. Zhang, J. Wang, J. Yan, and H. X. Tang, "17 000%/W second-harmonic conversion efficiency in single-crystalline aluminum nitride microresonators," Appl. Phys. Lett. **113**(13), 131102 (2018).
7. Y. Dumeige and P. Féron, "Whispering-gallery-mode analysis of phase-matched doubly resonant second-harmonic generation," Phys. Rev. A **74**(6), 063804 (2006).
8. P. Guillemé, M. Vallet, J. Stodolna, A. Ponchet, C. Cornet, A. Létoublon, P. Féron, O. Durand, Y. Léger, and Y. Dumeige, "Antiphase domain tailoring for combination of modal and 4¯ -quasi-phase matching in gallium phosphide microdisks," Opt. Express **24**(13), 14608 (2016).
9. P. S. Kuo, J. Bravo-Abad, and G. S. Solomon, "Second-harmonic generation using -quasi-phasematching in a GaAs whispering-gallery-mode microcavity," Nat. Commun. **5**(1), 3109 (2014).
10. A. D. Logan, M. Gould, E. R. Schmidgall, K. Hestroffer, Z. Lin, W. Jin, A. Majumdar, F. Hatami, A. W. Rodriguez, and K.-M. C. Fu, "400%/W second harmonic conversion efficiency in 14 μm-diameter gallium phosphide-on-oxide resonators," Opt. Express **26**(26), 33687 (2018).
11. I. Roland, M. Gromovyi, Y. Zeng, M. El Kurdi, S. Sauvage, C. Brimont, T. Guillet, B. Gayral, F. Semond, J. Y. Duboz, M. de Micheli, X. Checoury, and P. Boucaud, "Phase-matched second harmonic generation with on-chip GaN-on-Si microdisks," Sci. Rep. **6**(1), 34191 (2016).
12. M. Mitchell, A. C. Hryciw, and P. E. Barclay, "Cavity optomechanics in gallium phosphide microdisks," Appl. Phys. Lett. **104**(14), 141104 (2014).
13. M. K. Chin and S. T. Ho, "Design and Modeling of Waveguide-Coupled Single-Mode Microring Resonators," J. Lightwave Technol. **16**(8), 1433–1446 (1998).
14. S. Biasi, P. Guilleme, A. Volpini, G. Fontana, and L. Pavesi, "Time response of a microring resonator to a rectangular pulse in different coupling regimes," arXiv:1903.10747 [physics] (2019).
15. F. Turri, F. Ramiro-Manzano, I. Carusotto, M. Ghulinyan, G. Pucker, and L. Pavesi, "Wavelength Dependence of a Vertically Coupled Resonator-Waveguide System," J. Lightwave Technol. **34**(23), 5385–5390 (2016).
16. X. Lu, G. Moille, Q. Li, D. A. Westly, A. Singh, A. Rao, S.-P. Yu, T. C. Briles, S. B. Papp, and K. Srinivasan, "Efficient telecom-to-visible spectral translation through ultralow power nonlinear nanophotonics," Nat. Photonics **13**(9), 593–601 (2019).
17. G. Moille, G. Moille, Q. Li, Q. Li, T. C. Briles, T. C. Briles, S.-P. Yu, S.-P. Yu, T. Drake, T. Drake, X. Lu, X. Lu, A. Rao, A. Rao, D. Westly, S. B. Papp, S. B. Papp, K. Srinivasan, K. Srinivasan, and K. Srinivasan, "Broadband resonator-waveguide coupling for efficient extraction of octave-spanning microcombs," Opt. Lett. **44**(19), 4737–4740 (2019).
18. L. Chang, A. Boes, P. Pintus, J. D. Peters, M. Kennedy, X.-W. Guo, N. Volet, S.-P. Yu, S. B. Papp, and J. E. Bowers, "Strong frequency conversion in heterogeneously integrated GaAs resonators," APL Photonics **4**(3), 036103 (2019).
19. C. E. de Nobriga, G. D. Hobbs, W. J. Wadsworth, J. C. Knight, D. V. Skryabin, A. Samarelli, M. Sorel, and R. M. D. L. Rue, "Supermode dispersion and waveguide-to-slot mode transition in arrays of silicon-on-insulator waveguides," Opt. Lett. **35**(23), 3925–3927 (2010).
20. W. L. Bond, "Measurement of the Refractive Indices of Several Crystals," J. Appl. Phys. **36**(5), 1674–1677 (1965).
21. N. A. M. Yahya, W. H. Lim, S. W. Phang, H. Ahmad, R. Zakaria, and F. R. M. Adikan, "Curing Methods Yield Multiple Refractive Index of Benzocyclobutene Polymer Film," Sci. Technol. **5**(2), 163–165 (2011).
22. M. L. Gorodetsky and V. S. Ilchenko, "Optical microsphere resonators: optimal coupling to high-Q whispering-gallery modes," J. Opt. Soc. Am. B **16**(1), 147–154 (1999).
23. E. Mimoun, L. D. Sarlo, J.-J. Zondy, J. Dalibard, and F. Gerbier, "Sum-frequency generation of 589 nm light with near-unit efficiency," Opt. Express **16**(23), 18684–18691 (2008).
24. T. J. A. Kippenberg, "Nonlinear Optics in Ultra-high Q Whispering-Gallery Optical Microcavities," phd, California Institute of Technology (2004).
25. P. Guillemé, Y. Dumeige, J. Stodolna, M. Vallet, T. Rohel, A. Létoublon, C. Cornet, A. Ponchet, O. Durand, and Y. Léger, "Second harmonic generation in gallium phosphide microdisks on silicon: from strict $\bar{4}$ to random quasi-phase matching," Semicond. Sci. Technol. **32**(6), 065004 (2017).
26. J. B. Surya, X. Guo, C.-L. Zou, and H. X. Tang, "Control of second-harmonic generation in doubly resonant aluminum nitride microrings to address a rubidium two-photon clock transition," Opt. Lett. **43**(11), 2696–2699 (2018).
27. P. Guillemé, "Génération de seconde harmonique dans les microdisques de phosphure de gallium intégrés sur silicium," PhD, INSA Rennes (2016).